

Structures of TorsinA and its disease-mutant complexed with an activator reveal the molecular basis for primary dystonia

F. Esra Demircioglu¹, Brian A. Sosa¹, Jessica Ingram², Hidde L. Ploegh² & Thomas U. Schwartz¹

¹Department of Biology, Massachusetts Institute of Technology, Cambridge, Massachusetts 02139, USA

²Whitehead Institute for Biomedical Research, 9 Cambridge Center, Cambridge, Massachusetts 02142, USA

Abstract

The most common cause of early onset primary dystonia, a neuromuscular disease, is a glutamate deletion (ΔE) at position 302/303 of TorsinA, a AAA+ ATPase that resides in the endoplasmic reticulum. While the function of TorsinA remains elusive, the ΔE mutation is known to diminish binding of two TorsinA ATPase activators: lamina-associated protein 1 (LAP1) and its paralog, luminal domain like LAP1 (LULL1). Using a nanobody as a crystallization chaperone, we obtained a 1.4 Å crystal structure of human TorsinA in complex with LULL1. This nanobody likewise stabilized the weakened TorsinA ΔE -LULL1 interaction, which enabled us to solve its structure at 1.4 Å also. A comparison of these structures shows, in atomic detail, the subtle differences in activator interactions that separate the healthy from the diseased state. This information may provide a structural platform for drug development, as a small molecule that rescues TorsinA ΔE could serve as a cure for primary dystonia.

Introduction

Torsins belong to the AAA+ (ATPases associated with a variety of cellular activities) ATPase family, a functionally diverse group of enzymes, which are fueled by ATP hydrolysis. AAA+ ATPases organize in structurally distinct fashions and interact with various accessory elements to remodel their protein or nucleic acid substrates (Erzberger and Berger, 2006; Wendler et al., 2012; White and Lauring, 2007). Torsins are poorly understood AAA+ proteins with yet elusive functions and unknown substrates (Laudermilch and Schlieker, 2016; Rose et al., 2015). Among the five human torsins (TorsinA, TorsinB, Torsin2A, Torsin3A and Torsin4A), neuronally expressed TorsinA carries the most clinical significance since it is at the root of primary dystonia. Primary dystonia is a devastating neuromuscular disease that is predominantly caused by the deletion of glutamate 302 or 303 (ΔE) in TorsinA (Goodchild et al., 2005; Ozelius et al., 1997). The etiology of primary dystonia is poorly understood (Breakefield et al., 2008; Granata and Warner, 2010), and there is currently no known cure for it.

TorsinA is an unusual AAA+ ATPase, because, unlike any other family member (Erzberger and Berger, 2006; Laudermilch and Schlieker, 2016; Rose et al., 2015; White and Lauring, 2007), it is localized to the endoplasmic reticulum (ER) and the contiguous perinuclear space (PNS), and because it is not self-activated, but instead needs the AAA+-like proteins Lamina-associated protein 1 (LAP1) or Luminal domain like LAP1 (LULL1) to catalyze ATP hydrolysis (Brown et al., 2014; McCullough and Sundquist, 2014; Sosa et al., 2014). LAP1 is a type-II transmembrane protein which resides at the inner nuclear membrane (INM) through its association with nuclear lamina (Goodchild and Dauer, 2005). LULL1 is a LAP1 paralog, which localizes to the outer nuclear membrane (ONM) and the continuous ER, with its N-terminal portion protruding into the cytoplasm (Goodchild and Dauer, 2005). The structurally similar luminal domains of LAP1/LULL1 interact with TorsinA, and they provide an arginine finger to the TorsinA active site to facilitate torsin's ATP hydrolysis (Brown et al., 2014; Sosa et al., 2014). Arginine fingers are key structural motifs of AAA+ ATPases because they neutralize the transition state during ATP

hydrolysis (Wendler et al., 2012). Since torsins lack arginine fingers themselves, this activation mechanism through LAP1/LULL1 is likely critical for their function. As reported by several labs, the disease mutant TorsinA ΔE is compromised in binding to LAP1/LULL1 (Naismith et al., 2009; Zhao et al., 2013; Zhu et al., 2010). Clearly, this suggests that a probable cause of primary dystonia is the lack of activation of TorsinA. In line with this suggestion, LAP1 deletion shows a similar phenotype to Torsin ΔE , and contributes to disease pathology (Kim et al., 2010). To investigate the molecular basis for primary dystonia as a result of the glutamate 302/303 deletion in TorsinA, we took a structural approach. We obtained high-resolution crystal structures of TorsinA as well as TorsinA ΔE , each in complex with LULL1, using a nanobody as crystallization chaperone. These structures likely open a pathway toward rational, structure-based drug design against primary dystonia.

Results

TorsinA is a catalytically inactive AAA+ ATPase (Brown et al., 2014; Zhao et al., 2013), notoriously ill-behaved *in vitro*, primarily due to its limited solubility and stability. We partially overcame these problems by stabilizing an ATP-trapped E171Q mutant of human TorsinA (residues 51-332) by co-expressing it with the luminal activation domain of human LULL1 (residues 233-470). This resulted in a better behaved heterodimeric complex (Figure 1A), which, however, was still recalcitrant to our crystallization efforts. To facilitate crystallization, we isolated a nanobody (VHH-BS2) from an alpaca immunized with the TorsinA_{EQ}-LULL1 complex. A stable, heterotrimeric complex of TorsinA_{EQ}-LULL1-VHH-BS2 was readily crystallized in the presence of ATP. We collected a 1.4 Å dataset and solved the structure by molecular replacement, using the LULL1-homolog LAP1 and a VHH template as search models (Sosa et al., 2014) (Materials and Methods, Table 1). TorsinA_{EQ} adopts a typical AAA+ ATPase fold (Figure 1B, Figure 1 – figure supplement 1). The N-terminal nucleotide-binding or large domain

(residues 55-271) is composed of a central five-stranded, parallel β -sheet surrounded by 8 α -helices. A small three-helix bundle at its C-terminus (residues 272-332), forms critical contacts with LULL1. An ATP molecule is bound in the manner characteristic of P-loop NTPases (Wendler et al., 2012). The Walker A and B motifs are positioned to mediate the requisite nucleotide interactions, with sensor 1 and sensor 2 regions sensing the γ -phosphate and thus the nucleotide state (Figure 1C). The luminal LULL1 activation domain (residues 236-470) adopts an AAA+-like conformation, very similar to its paralog LAP1 (rmsd 1.05 Å over 213 C α positions, Figure 1 – figure supplement 1). The AAA+-like domain comprises a central β -sheet embedded within six α -helices (Figure 1B). A C-terminal small domain is not present. Similar to LAP1, an intramolecular disulfide bond forms at the C terminus of LULL1, between conserved residues C310 and C468 (Figure 1 – figure supplements 1 and 3). Characteristically, LULL1 lacks nucleotide binding due to the absence of Walker A and B motifs (Sosa et al., 2014). LULL1 forms a composite nucleotide-binding site with TorsinA by providing arginine residue 449 ('arginine finger') at the base of helix α 5 (Figure 1C). The arginine finger activates ATP hydrolysis by TorsinA (Brown et al., 2014; Sosa et al., 2014). The small domain of TorsinA, including helix α 7 featuring glutamates 302 and 303, is intimately involved in LULL1 binding. Nanobody VHH-BS2 binds both TorsinA and LULL1 at a shallow groove (Figure 1B, Figure 1 – figure supplement 4). Nanobodies contain three complementarity determining regions (CDRs), with CDR3 most often making critical contacts with the antigen (Muyldermans, 2013). Indeed, the long CDR3 of VHH-BS2 (residues 97-112) is the main binding element in the complex. AAA+ ATPases are organized into a number of structurally defined clades (Erzberger and Berger, 2006; Iyer et al., 2004), distinguished by shared structural elements. Comparison with other AAA+ ATPase structures shows that TorsinA fits best into a clade that also contains the bacterial proteins HslU, ClpA/B, ClpX, and Lon (HCLR clade), all of which are involved in protein degradation or remodeling (Erzberger and Berger, 2006). These AAA+ family members share a

114 β -hairpin insertion that precedes the sensor-I region (Figure 1 – figure supplement 1). TorsinA
115 also contains this structural element, but it adopts a distinctly different orientation compared to
116 other members of the clade; however, the pre-sensor I region may be affected by crystal
117 packing in our structure. Two other distinct regions are present. The protein degrading or
118 remodeling AAA+ ATPases all form hexameric rings with a central pore (Hanson and
119 Whiteheart, 2005; Olivares et al., 2016; White and Luring, 2007). ‘Pore loops’ in each subunit,
120 conserved elements positioned between strand $\beta 2$ and helix $\alpha 2$, are critical for threading the
121 protein substrates through the ring (Sauer and Baker, 2011). Torsins are devoid of a pore loop
122 consensus motif (Figure 1 – figure supplements 2 and 5). TorsinA has two cysteines (Cys280,
123 and Cys 319, which is part of the sensor-II motif), positioned near the adenine base of the ATP
124 molecule (Figure 1D-F). These cysteines do not form a disulfide bridge in our structure.
125 However, the conservation of Cys280 and the Gly-Cys-Lys sensor-II motif at position 318-320
126 (Figure 1 – figure supplements 2 and 5) indicates an important functional role. A redox activity
127 as part of the ATPase cycle therefore seems highly likely, as has been previously speculated
128 (Zhu et al., 2008; 2010).

129 The interaction of TorsinA with its ATPase activators LULL1 and LAP1 is of particular
130 importance, as a prominent mutation causing primary dystonia--the deletion of glutamate 302 or
131 303--weakens these interaction (Naismith et al., 2009; Zhao et al., 2013; Zhu et al., 2010). But
132 why and how? The TorsinA-LULL1 interface extends over an area of 1527 Å². The main
133 structural elements involved in this interaction are the nucleotide-binding region as well as the
134 small domain of TorsinA, and helices $\alpha 0$, $\alpha 2$, $\alpha 4$ and $\alpha 5$ of LULL1 (Figure 1, Figure 1 – figure
135 supplements 2 and 3, Figure 2A). The exact position of the small domain of TorsinA relative to
136 the large domain is likely dictated by the sensor II motif, preceding $\alpha 8$, which directly contacts
137 the γ -phosphate of ATP through Lys 320, thus serving as an anchor point. A switch to ADP
138 presumably weakens this connection, such that the small domain would become more loosely

attached to the large domain. This could explain the observed ATP-dependency of LAP1/LULL1 binding (Goodchild and Dauer, 2005; Naismith et al., 2009; Zhao et al., 2013; Zhu et al., 2010). Within the small domain, helix $\alpha 7$, the following loop, and the terminal helix $\alpha 8$ contain all the critical residues. Glutamate 302 and 303 are positioned at the very end of helix $\alpha 7$, and both are involved in TorsinA contacts. Specifically, Glu 303 forms a prominent charge interaction with Arg 276 of LULL1. TorsinA Lys113 – LULL1 Glu385, TorsinA Asp316 - LULL1 Arg419, TorsinA Lys317 - LULL1 Glu415 are additional charge interactions.

To investigate the atomic details of the weakened binding of TorsinA ΔE to LAP1/LULL1, and thus the molecular basis of primary dystonia, we made use of the observation that VHH-BS2 also stabilizes the TorsinA_{EQ} ΔE (ATP)-LULL1 interaction. We were able to crystallize TorsinA_{EQ} ΔE (ATP)-LULL1-VHH-BS2 and determine its structure at a resolution of 1.4 Å. Not surprisingly, the overall structure is almost identical to the wild-type protein (0.34 Å rmsd over 274 C α atoms for TorsinA, 0.26 Å rmsd over 229 C α atoms for LULL1), except for critical differences in the TorsinA-LULL1 interface (Figure 2A). The principal difference is that helix $\alpha 7$ is shortened due to the missing Glu 303, with a slight--but significant--restructuring of the loop that follows to establish the connection with helix $\alpha 8$. For future reference, we suggest renaming the ΔE mutation $\Delta E303$, rather than $\Delta E302/303$, since the position of Glu 302 is effectively unchanged. In the dystonia mutant, the TorsinA Glu 303 – LULL1 Arg 276 charge interaction is lost, and the hydrogen-bonding network involving TorsinA Glu 302, Phe 306 and Arg312, as well as LULL1 Arg412 and Glu416 is disrupted (Figure 2A). To determine the importance of different TorsinA residues for LULL1 binding, we performed a co-purification assay (Figure 2B, C). His-tagged, ATP-trapped TorsinA_{EQ} (residues 51-332) and mutants thereof were recombinantly co-expressed with LULL1 (residues 233-470), but without VHH-BS2, in bacteria. Binding was tested in a co-purification assay using Ni-affinity. The TorsinA_{EQ} $\Delta E303$ mutation abolishes binding in this assay, as expected (Figure 2B). Since unbound TorsinA_{EQ} is largely

insoluble, absence of binding is not registered as an appearance of TorsinA_{EQ} alone, but rather as a lack of eluted protein complex altogether. Eliminating the salt bridge between TorsinA Glu303 and LULL1 Arg276 does not disrupt the TorsinA-LULL1 interaction (Figure 2B). However, Δ Met304 and Δ Thr305 both phenocopy Δ E303 in abolishing LULL1 binding (Figure 2C). This is in full agreement with published *in vivo* data using similar mutants (Goodchild and Dauer, 2004). The intricate network of interactions of the α 7- α 8 loop of TorsinA is crucial for LULL1 binding. Since the Δ E mutation causes a local change within the small domain of TorsinA rather than protein misfolding, it may be possible to rescue binding by developing a small molecule that resurrects the weakened TorsinA Δ E-LAP1/LULL1 interaction.

Although TorsinA Δ E303 is the most prevalent mutation that causes primary dystonia, it is not the only one (Laudermilch and Schlieker, 2016; Rose et al., 2015). We examined the structural consequence of all known mutations (Figure 2 – figure supplement 1, Table 2). Based on our structural data, we strongly predict that most mutations likely cause protein misfolding or they weaken or abolish LAP1/LULL1 binding. Conversely, the two dystonia-mutations found in LAP1 presumably affect torsin interaction. Our structural data therefore clearly supports the hypothesis that improper torsin activation is the likely cause of primary dystonia (Kim et al., 2010).

Discussion

The biological function of TorsinA remains enigmatic (Granata et al., 2011; Jokhi et al., 2013; Liang et al., 2014; Nery et al., 2008; 2011). Because TorsinA belongs to the AAA+ ATPase superfamily, with specific homology to the bacterial proteins HslU, ClpX, ClpA/B and Lon, it is generally assumed that TorsinA is involved in protein remodeling or protein degradation (Laudermilch and Schlieker, 2016; Rose et al., 2015). However, a substrate of TorsinA has yet to be identified.

The TorsinA structure enables a more thorough comparison to other AAA+ ATPases, particularly with regard to the functionally relevant oligomerization state. After the discovery that LAP1/LULL1 are Arg-finger containing TorsinA activators with a AAA+-like structure, it seemed reasonable to suggest that TorsinA and LAP1/LULL1 likely form heterohexameric rings ((TorsinA-ATP-LAP1/LULL1)₃) in order to function (Brown et al., 2014; Sosa et al., 2014). However, the predominant oligomeric form of recombinant TorsinA-ATP-LAP1/LULL1 complex *in vitro* and in solution is the heterodimer (Brown et al., 2014; Sosa et al., 2014). In addition, torsin variants have been reported to occur in various oligomeric forms as detected by Blue Native PAGE (BN-PAGE) (Goodchild et al., 2015; Jungwirth et al., 2010; Vander Heyden et al., 2009). Our structure now raises doubts about the physiological relevance of a heterohexameric ring (Figure 3). First, we note that the small domain of TorsinA is essential for LAP1/LULL1 binding (Figure 2C). This is reminiscent of the related HCLR AAA+ clade members where the small domain is known to be critical for hexamerization (Bochtler et al., 2000; Mogk et al., 2003). The importance of the small domain for oligomerization in the context of torsins has also been discussed recently (Rose et al., 2015). Neither LAP1 nor LULL1 harbor a small domain, arguing against formation of a stable heteromeric ring, or, alternatively, suggesting a ring of substantially different architecture. Second, ring formation is important for AAA+ ATPases that thread their protein substrate through a central pore for refolding or for degradation. This central pore is lined with conserved 'pore loops' that are essential for function (White and Lauring, 2007). Neither TorsinA and its homologs, nor LAP1/LULL1 have 'pore loop' equivalents (Figure 1 – figure supplement 5). TorsinA is therefore unlikely to actually employ a peptide threading mechanism that involves a central pore. Third, the surface conservation of LAP1/LULL1 also argues against a heteromeric ring assembly. Although the catalytic, ATP-containing interface with TorsinA is well-conserved, the presumptive non-catalytic, nucleotide-free interface is not (Figure 3B). Importantly and in contrast to LAP1/LULL1, the same analysis for TorsinA shows that its 'backside' is conserved. TorsinA may therefore interact in homotypic fashion with

TorsinA, with other torsin homologs, or even with an additional, yet unidentified protein. This could mean that the previously observed hexameric assemblies (Goodchild et al., 2015; Jungwirth et al., 2010; Sosa et al., 2014) may only contain one LAP1/LULL1 unit, and multiple torsin units, a property that the employed assays would not have differentiated. It is also possible, that the reported hexameric assemblies reflect a vestigial, yet physiologically irrelevant property, perhaps just of the evolutionary origin of the Torsin-LAP1/LULL1 system. Taking all the existing data into account, it is suggestive that TorsinA may be an exceptional AAA+ ATPase in that it simply acts as a heterodimer, together with LAP1 or LULL1 functioning as an activator. As long as the biological function and the substrate for TorsinA are unclear, however, the physiologically relevant oligomeric state of TorsinA ultimately remains a matter of speculation. Given the unique properties of TorsinA, keeping an open mind about TorsinA assembly into its functional state is called for, as it may well differ more than anticipated from well-studied AAA+ ATPase systems.

The observation that the nanobody VHH-BS2 stabilizes the TorsinA Δ E303-LULL1 suggests that it could possibly be used directly as a therapeutic. After all, it could directly rescue TorsinA activity. There are, however, at least two major problems. First, VHH-BS2 only recognizes the TorsinA- (or TorsinA Δ E303-) LULL1 complex, but not the homologous TorsinA-LAP1 complex. The function of LULL1 is still poorly understood, but a knockdown does not generate an NE blebbing phenotype (Goodchild et al., 2015; Turner et al., 2015; Vander Heyden et al., 2009), which is symptomatic for a TorsinA knockout (Goodchild et al., 2005) or a LAP1 knockdown (Kim et al., 2010). Therefore, resurrecting activation of TorsinA Δ E303 via LULL1 is unlikely to ameliorate the dystonia phenotype. Furthermore, the nanobody interaction site on the TorsinA-LULL1 interface is very likely oriented toward the ER membrane, which can be inferred from the relative positions of the membrane anchor of LULL1 and the hydrophobic,

likely membrane-proximal N-terminal region of TorsinA. These topological restraints suggest that the nanobody will not bind *in vivo*, but that it is of significant use for *in vitro* studies.

Materials and Methods

Constructs, protein expression and purification

DNA sequences encoding human TorsinA (residues 51-332) and the luminal domain of human LULL1 (residues 233-470) were cloned into a modified ampicillin resistant pETDuet-1 vector (EMD Millipore). TorsinA, N-terminally fused with a human rhinovirus 3C protease cleavable 10xHis-7xArg tag, was inserted into the first multiple cloning site (MCS), whereas the untagged LULL1 was inserted into the second MCS. Mutations on TorsinA and LULL1 were introduced by site-directed mutagenesis. The untagged VHH-BS2 nanobody was cloned into a separate, modified kanamycin resistant pET-30b(+) vector (EMD Biosciences).

To co-express TorsinA (EQ or EQ/ Δ E), LULL1 and VHH-BS2 for crystallization, the *E. coli* strain LOBSTR(DE3) RIL (Kerafast) (Andersen et al., 2013) was co-transformed with the two constructs described above. Cells were grown at 37°C in lysogeny broth (LB) medium supplemented with 100 $\mu\text{g ml}^{-1}$ ampicillin, 25 $\mu\text{g ml}^{-1}$ kanamycin and 34 $\mu\text{g ml}^{-1}$ chloramphenicol until an optical density (OD_{600}) of 0.6-0.8 was reached, shifted to 18°C for 20 min, and induced overnight at 18°C with 0.2 mM isopropyl β -D-1-thiogalactopyranoside (IPTG). The bacterial cultures were harvested by centrifugation, suspended in lysis buffer (50 mM HEPES/NaOH pH 8.0, 400 mM NaCl, 40 mM imidazole, 10 mM MgCl_2 , and 1 mM ATP) and lysed with a cell disruptor (Constant Systems). The lysate was immediately mixed with 0.1 M phenylmethanesulfonyl fluoride (PMSF) (50 μl per 10 ml lysate) and 250 units of TurboNuclease (Eton Bioscience), and cleared by centrifugation. The soluble fraction was gently mixed with Ni-Sepharose 6 Fast Flow (GE Healthcare) resin for 30 min at 4°C. After washing with the lysis buffer, bound protein was eluted in elution buffer (10 mM HEPES/NaOH pH 8.0, 150 mM NaCl,

300 mM imidazole, 10 mM MgCl₂, and 1 mM ATP). The eluted protein complex was immediately purified by size exclusion chromatography on a Superdex S200 column (GE Healthcare) equilibrated in running buffer (10 mM HEPES/NaOH pH 8.0, 150 mM NaCl, 10 mM MgCl₂, and 0.5 mM ATP). Following the tag removal by 10xHis-7xArg-3C protease, the fusion tags and the protease were separated from the complex by cation-exchange chromatography on a HiTrapS column (GE Healthcare) using a linear NaCl gradient. The flow-through from the cation-exchange chromatography, containing the protein complex, was purified again by size exclusion chromatography on a Superdex S200 column as at the previous step.

For the non-structural analysis of TorsinA and LULL1 variants, the pETDuet-1-based expression plasmid was transformed into LOBSTR(DE3) RIL cells without co-expressing nanobody VHH-BS2. Ni²⁺-affinity purification was performed as described above and bound protein was eluted. Aliquots from the Ni²⁺-eluate and the total lysate were collected and analyzed by SDS-PAGE gel electrophoresis.

Crystallization

Purified TorsinA_{EQ}-LULL1-VHH-BS2 and TorsinA_{EQΔE}-LULL1-VHH-BS2 complexes were concentrated up to 4-4.5 mg/ml and supplemented with 2 mM ATP prior to crystallization. The TorsinA_{EQ} containing complex crystallized in 13% (w/v) polyethylene glycol (PEG) 6000, 5% (v/v) 2-Methyl-2,4-pentanediol, and 0.1 M MES pH 6.5. The TorsinA_{EQΔE} containing complex crystallized in 19% (w/v) PEG 3350, 0.2 M AmSO₄, and 0.1 M Bis-Tris-HCl pH 6.5. Crystals of both complexes grew at 18°C in hanging drops containing 1 μl of protein and 1 μl of mother liquor. Clusters of diffraction quality, rod-shaped crystals formed within 3-5 days. Single crystals were briefly soaked in mother liquor supplemented with 20% (v/v) glycerol for cryoprotection and flash-frozen in liquid nitrogen.

Data collection and structure determination

289 X-ray data were collected at NE-CAT beamline 24-ID-C at Argonne National Laboratory. Data
290 reduction was performed with the HKL2000 package (Otwinowski and Minor, 1997), and all
291 subsequent data-processing steps were carried out using programs provided through SBGrid
292 (Morin et al., 2013). The structure of the TorsinA_{EQ}-LULL1-VHH-BS2 complex was solved by
293 molecular replacement (MR) using the Phaser-MR tool from the PHENIX suite (Adams et al.,
294 2010). A three-part MR solution was easily obtained using a sequential search for models of
295 LULL1, VHH-BS2, and TorsinA. The LULL1 model was generated based on the published
296 human LAP1 structure (PDB 4TVS, chain A), using the Sculptor utility of the PHENIX suite
297 (LULL1₂₄₁₋₄₇₀ and LAP1₃₅₆₋₅₈₃ share 64% sequence identity). The VHH-BS2 model was based on
298 VHH-BS1 (PDB 4TVS, chain a) after removing the complementarity determining regions
299 (CDRs). The poly-Ala model of TorsinA was generated based on *E. coli* ClpA (PDB 1R6B) using
300 the MODELLER tool of the HHpred server (Söding et al., 2005). The asymmetric unit contains
301 one TorsinA_{EQ}-LULL1-VHH-BS2 complex. Iterative model building and refinement steps
302 gradually improved the electron density maps and the model statistics. The stereochemical
303 quality of the final model was validated by Molprobity (Chen et al., 2010). TorsinA_{EQ}ΔE-LULL1-
304 VHH-BS2 crystallized in the same unit cell. Model building was carried starting from a truncated
305 TorsinA_{EQ}-LULL1-VHH-BS2 structure. All manual model building steps were carried out with
306 Coot (Emsley et al., 2010), and *phenix.refine* was used for iterative refinement. Two alternate
307 conformations of a loop in LULL1 (residues 428-438) were detected in the F_o-F_c difference
308 electron density maps of both structures, and they were partially built. For comparison, the
309 cysteine residues of TorsinA at the catalytic site (residues 280 and 319 in the TorsinA_{EQ}
310 structure) were built in the reduced and the oxidized states, respectively. Building them as
311 oxidized, disulfide-bridged residues consistently produced substantial residual F_o-F_c difference
312 density, which disappeared assuming a reduced state. Statistical parameters of data collection
313 and refinement are all given in Table 1. Structure figures were created in PyMOL (Schrödinger
314 LLC).

315

316 **Bioinformatic analysis**

317 Torsin and LAP1/LULL1 sequences were obtained via PSI-BLAST (Altschul et al., 1997) and
318 Backphyre searches (Kelley and Sternberg, 2009). Transmembrane domains were predicted
319 using the HMMTOP tool (Tusnády and Simon, 2001). LAP1/LULL1 proteins were distinguished
320 based on the calculated isoelectric point (pI) of their extra-luminal portions. The intranuclear
321 domain of LAP1 has a characteristically high pI of ~8.5-10 due to a clustering of basic residues,
322 while the cytoplasmic domain of LULL1 is distinctively more acidic. Multiple sequence
323 alignments were performed using MUSCLE (Edgar, 2004), and visualized by Jalview
324 (Waterhouse et al., 2009). To illustrate evolutionary conservation on TorsinA and LULL1
325 surfaces, conservation scores for each residue were calculated using the ConSurf server with
326 default parameters (Glaser et al., 2003).

327 The sequences, which were used to generate the multiple sequence alignments, were also
328 used for preparing the sequence logos of Torsins and LAP1/LULL1 in Figure 1 – figure
329 supplement 5. To obtain the sequence logo of the HCLR clade AAA+ ATPases, *Escherichia coli*
330 ClpA-D2 (residues 458-758), *Escherichia coli* ClpB-D2 (residues 568-857), *Bacillus subtilis*
331 ClpE-D2 (residues 409-699), *Saccharomyces cerevisiae* Hsp104-D2 (residues 578-868),
332 *Escherichia coli* HslU (residues 13-443), *Bacillus subtilis* HslU (residues 15-455), *Streptomyces*
333 *coelicolor* ClpX (residues 71-409), *Drosophila melanogaster* ClpX (residues 199-634),
334 *Escherichia coli* Lon (residues 320-580), *Caenorhabditis elegans* Lon (residues 476-771),
335 *Thermus thermophilus* ClpB-D2 (residues 536-845), *Escherichia coli* ClpX (residues 64-403),
336 *Helicobacter pylori* ClpX (residues 77-430), *Haemophilus influenza* HslU (1-444), *Bacillus*
337 *subtilis* Lon (residues 300-590), *Bacillus subtilis* ClpC-D2 (residues 486-802), *Saccharomyces*
338 *cerevisiae* Hsp78-D2 (residues 482-794) and *Arabidopsis thaliana* Hsp101-D2 (residues 547-
339 849) sequences were used. All sequence logos were generated using WebLogo (Crooks et al.,
340 2004).

Generation and selection of nanobodies

Purified human TorsinA_{EQ}-LULL1 complex was injected into a male alpaca (*Lama pacos*) for immunization. Generation and screening of nanobodies was carried out as previously described (Sosa et al., 2014). Each of the selected nanobodies was subcloned into a pET-30b(+) vector with a C-terminal His₆-tag. Each nanobody was bacterially expressed and Ni²⁺-affinity purified essentially as described (see above). Different from the TorsinA-containing preparations, MgCl₂ and ATP were eliminated from all buffer solutions. The Ni²⁺-eluate was purified via size exclusion chromatography on a Superdex S75 column (GE Healthcare) in running buffer (10 mM HEPES/NaOH pH 8.0, 150 mM NaCl). Nanobody binding was validated by size exclusion chromatography on a 10/300 Superdex S200 column in 10 mM HEPES/NaOH pH 8.0, 150 mM NaCl, 10 mM MgCl₂ and 0.5 mM ATP. Equimolar amounts of TorsinA_{EQ}-LULL1 and TorsinA_{EQ}-LULL1-VHH were loaded and nanobody binding was monitored by a shift in the elution profile and via SDS-PAGE analysis. After validating VHH-BS2 interaction with TorsinA_{EQ}-LULL1, the C-terminal His₆-tag of VHH-BS2 was removed from the pET-30b(+) vector for co-purification experiments.

Acknowledgements

The authors thank Ulrike Kutay for many helpful discussions pertinent to this study. The work in the Schwartz lab was supported by the Foundation for Dystonia Research and a National Institutes of Health grant (AR065484). Work in the lab of H.L.P. was supported by an NIH Director's Pioneer award. Structural data is based upon research conducted at the Northeastern Collaborative Access Team beamlines, which are funded by the National Institute of General Medical Sciences from the National Institutes of Health (P41 GM103403). This research used resources of the Advanced Photon Source, a U.S. Department of Energy (DOE) Office of Science User Facility operated for the DOE Office of Science by Argonne National Laboratory under Contract No. DE-AC02-06CH11357.

Author Contributions

FED generated expression constructs, performed biochemical tests, crystallized protein and solved the crystal structures; BAS screened and cloned nanobodies; JI, and HLP helped with nanobody generation and contributed to the manuscript; FED and TUS interpreted the structure and wrote the manuscript. TUS supervised the project.

Competing Interests

FED, BAS, and TUS have filed a provisional patent application protecting the use of the crystal structures (U.S.P.T.O. No. 62/330,683).

References

388 Adams, P.D., Afonine, P.V., Bunkóczi, G., Chen, V.B., Davis, I.W., Echols, N., Headd, J.J.,
 389 Hung, L.-W., Kapral, G.J., Grosse-Kunstleve, R.W., et al. (2010). PHENIX: a comprehensive
 390 Python-based system for macromolecular structure solution. *Acta Crystallogr. D Biol. Crystallogr.*
 391 66, 213–221.

392 Altschul, S.F., Madden, T.L., Schäffer, A.A., Zhang, J., Zhang, Z., Miller, W., and Lipman, D.J.
 393 (1997). Gapped BLAST and PSI-BLAST: a new generation of protein database search
 394 programs. *Nucleic Acids Res.* 25, 3389–3402.

395 Andersen, K.R., Leksa, N.C., and Schwartz, T.U. (2013). Optimized *E. coli* expression strain
 396 LOBSTR eliminates common contaminants from His-tag purification. *Proteins* 81, 1857–1861.

397 Bochtler, M., Hartmann, C., Song, H.K., Bourenkov, G.P., Bartunik, H.D., and Huber, R. (2000).
 398 The structures of HslU and the ATP-dependent protease HslU-HslV. *Nature* 403, 800–805.

399 Breakefield, X.O., Blood, A.J., Li, Y., Hallett, M., Hanson, P.I., and Standaert, D.G. (2008). The
 400 pathophysiological basis of dystonias. *Nat. Rev. Neurosci.* 9, 222–234.

401 Brown, R.S.H., Zhao, C., Chase, A.R., Wang, J., and Schlieker, C. (2014). The mechanism of
 402 Torsin ATPase activation. *Proc. Natl. Acad. Sci. U.S.A.* 111, E4822–E4831.

403 Calakos, N., Patel, V.D., Gottron, M., Wang, G., Tran-Viet, K.-N., Brewington, D., Beyer, J.L.,
 404 Steffens, D.C., Krishnan, R.R., and Züchner, S. (2010). Functional evidence implicating a novel
 405 TOR1A mutation in idiopathic, late-onset focal dystonia. *J. Med. Genet.* 47, 646–650.

406 Chen, V.B., Arendall, W.B., Headd, J.J., Keedy, D.A., Immormino, R.M., Kapral, G.J., Murray,
 407 L.W., Richardson, J.S., and Richardson, D.C. (2010). MolProbity: all-atom structure validation
 408 for macromolecular crystallography. *Acta Crystallogr. D Biol. Crystallogr.* 66, 12–21.

409 Cheng, F.-B., Feng, J.-C., Ma, L.-Y., Miao, J., Ott, T., Wan, X.-H., and Grundmann, K. (2014).
 410 Combined occurrence of a novel TOR1A and a THAP1 mutation in primary dystonia. *Mov.*
 411 *Disord.* 29, 1079–1083.

412 Crooks, G.E., Hon, G., Chandonia, J.-M., and Brenner, S.E. (2004). WebLogo: a sequence logo
 413 generator. *Genome Res.* 14, 1188–1190.

414 Dobričić, V., Kresojević, N., Žarković, M., Tomić, A., Marjanović, A., Westenberger, A.,
 415 Cvetković, D., Svetel, M., Novaković, I., and Kostić, V.S. (2015). Phenotype of non-
 416 c.907_909delGAG mutations in TOR1A: DYT1 dystonia revisited. *Parkinsonism Relat. Disord.*
 417 21, 1256–1259.

418 Dorboz, I., Coutelier, M., Bertrand, A.T., Caberg, J.-H., Elmaleh-Bergès, M., Lainé, J., Stevanin,
 419 G., Bonne, G., Boespflug-Tanguy, O., and Servais, L. (2014). Severe dystonia, cerebellar
 420 atrophy, and cardiomyopathy likely caused by a missense mutation in TOR1AIP1. *Orphanet J*
 421 *Rare Dis* 9, 174.

422 Edgar, R.C. (2004). MUSCLE: a multiple sequence alignment method with reduced time and
 423 space complexity. *BMC Bioinformatics* 5, 113.

424 Emsley, P., Lohkamp, B., Scott, W.G., and Cowtan, K. (2010). Features and development of
 425 Coot. *Acta Crystallogr. D Biol. Crystallogr.* 66, 486–501.

426 Erzberger, J.P., and Berger, J.M. (2006). Evolutionary relationships and structural mechanisms
 427 of AAA+ proteins. *Annu Rev Biophys Biomol Struct* 35, 93–114.

428 Glaser, F., Pupko, T., Paz, I., Bell, R.E., Bechor-Shental, D., Martz, E., and Ben-Tal, N. (2003).
 429 ConSurf: identification of functional regions in proteins by surface-mapping of phylogenetic
 430 information. *Bioinformatics* 19, 163–164.

431 Goodchild, R.E., and Dauer, W.T. (2004). Mislocalization to the nuclear envelope: an effect of
 432 the dystonia-causing torsinA mutation. *Proc. Natl. Acad. Sci. U.S.a.* 101, 847–852.

433 Goodchild, R.E., Kim, C.E., and Dauer, W.T. (2005). Loss of the dystonia-associated protein
 434 torsinA selectively disrupts the neuronal nuclear envelope. *Neuron* 48, 923–932.

435 Goodchild, R.E., and Dauer, W.T. (2005). The AAA+ protein torsinA interacts with a conserved
 436 domain present in LAP1 and a novel ER protein. *J. Cell Biol.* 168, 855–862.

437 Goodchild, R.E., Buchwalter, A.L., Naismith, T.V., Holbrook, K., Billion, K., Dauer, W.T., Liang,
 438 C.-C., Dear, M.L., and Hanson, P.I. (2015). Access of torsinA to the inner nuclear membrane is
 439 activity dependent and regulated in the endoplasmic reticulum. *J. Cell. Sci.* 128, 2854–2865.

440 Granata, A., and Warner, T.T. (2010). The role of torsinA in dystonia. *Eur. J. Neurol.* 17 Suppl 1,
 441 81–87.

442 Granata, A., Koo, S.J., Haucke, V., Schiavo, G., and Warner, T.T. (2011). CSN complex
 443 controls the stability of selected synaptic proteins via a torsinA-dependent process. *Embo J.* 30,
 444 181–193.

445 Hanson, P.I., and Whiteheart, S.W. (2005). AAA+ proteins: have engine, will work. *Nat. Rev.*
 446 *Mol. Cell Biol.* 6, 519–529.

447 Iyer, L.M., Leipe, D.D., Koonin, E.V., and Aravind, L. (2004). Evolutionary history and higher
 448 order classification of AAA+ ATPases. *J. Struct. Biol.* 146, 11–31.

449 Jokhi, V., Ashley, J., Nunnari, J., Noma, A., Ito, N., Wakabayashi-Ito, N., Moore, M.J., and
 450 Budnik, V. (2013). Torsin mediates primary envelopment of large ribonucleoprotein granules at
 451 the nuclear envelope. *Cell Rep* 3, 988–995.

452 Jungwirth, M., Dear, M.L., Brown, P., Holbrook, K., and Goodchild, R. (2010). Relative tissue
 453 expression of homologous torsinB correlates with the neuronal specific importance of DYT1
 454 dystonia-associated torsinA. *Hum. Mol. Genet.* 19, 888–900.

455 Kamm, C., Fischer, H., Garavaglia, B., Kullmann, S., Sharma, M., Schrader, C., Grundmann, K.,
 456 Klein, C., Borggraefe, I., Lobsien, E., et al. (2008). Susceptibility to DYT1 dystonia in European
 457 patients is modified by the D216H polymorphism. *Neurology* 70, 2261–2262.

458 Kayman-Kurekci, G., Talim, B., Korkusuz, P., Sayar, N., Sarioglu, T., Oncel, I., Sharafi, P.,
 459 Gundesli, H., Balci-Hayta, B., Purali, N., et al. (2014). Mutation in TOR1AIP1 encoding LAP1B
 460 in a form of muscular dystrophy: a novel gene related to nuclear envelopopathies. *Neuromuscul.*
 461 *Disord.* 24, 624–633.

462 Kelley, L.A., and Sternberg, M.J.E. (2009). Protein structure prediction on the Web: a case

study using the Phyre server. *Nat Protoc* 4, 363–371.

Kim, C.E., Perez, A., Perkins, G., Ellisman, M.H., and Dauer, W.T. (2010). A molecular mechanism underlying the neural-specific defect in torsinA mutant mice. *Proc. Natl. Acad. Sci. U.S.A.* 107, 9861–9866.

Kock, N., Naismith, T.V., Boston, H.E., Ozelius, L.J., Corey, D.P., Breakefield, X.O., and Hanson, P.I. (2006). Effects of genetic variations in the dystonia protein torsinA: identification of polymorphism at residue 216 as protein modifier. *Hum. Mol. Genet.* 15, 1355–1364.

Laudermilch, E., and Schlieker, C. (2016). Torsin ATPases: structural insights and functional perspectives. *Curr. Opin. Cell Biol.* 40, 1–7.

Leung, J.C., Klein, C., Friedman, J., Vieregge, P., Jacobs, H., Doheny, D., Kamm, C., DeLeon, D., Pramstaller, P.P., Penney, J.B., et al. (2001). Novel mutation in the TOR1A (DYT1) gene in atypical early onset dystonia and polymorphisms in dystonia and early onset parkinsonism. *Neurogenetics* 3, 133–143.

Liang, C.-C., Tanabe, L.M., Jou, S., Chi, F., and Dauer, W.T. (2014). TorsinA hypofunction causes abnormal twisting movements and sensorimotor circuit neurodegeneration. *J. Clin. Invest.* 124, 3080–3092.

McCullough, J., and Sundquist, W.I. (2014). Putting a finger in the ring. *Nat. Struct. Mol. Biol.* 21, 1025–1027.

Mogk, A., Schlieker, C., Strub, C., Rist, W., Weibezahn, J., and Bukau, B. (2003). Roles of individual domains and conserved motifs of the AAA+ chaperone ClpB in oligomerization, ATP hydrolysis, and chaperone activity. *J. Biol. Chem.* 278, 17615–17624.

Morin, A., Eisenbraun, B., Key, J., Sanschagrin, P.C., Timony, M.A., Ottaviano, M., and Sliz, P. (2013). Collaboration gets the most out of software. *Elife* 2, e01456.

Muyldermans, S. (2013). Nanobodies: natural single-domain antibodies. *Annu. Rev. Biochem.* 82, 775–797.

Naismith, T.V., Dalal, S., and Hanson, P.I. (2009). Interaction of torsinA with its major binding partners is impaired by the dystonia-associated DeltaGAG deletion. *J. Biol. Chem.* 284, 27866–27874.

Nery, F.C., Zeng, J., Niland, B.P., Hewett, J., Farley, J., Irimia, D., Li, Y., Wiche, G., Sonnenberg, A., and Breakefield, X.O. (2008). TorsinA binds the KASH domain of nesprins and participates in linkage between nuclear envelope and cytoskeleton. *J. Cell. Sci.* 121, 3476–3486.

Nery, F.C., Armata, I.A., Farley, J.E., Cho, J.A., Yaqub, U., Chen, P., da Hora, C.C., Wang, Q., Tagaya, M., Klein, C., et al. (2011). TorsinA participates in endoplasmic reticulum-associated degradation. *Nat Commun* 2, 393.

Olivares, A.O., Baker, T.A., and Sauer, R.T. (2016). Mechanistic insights into bacterial AAA+ proteases and protein-remodelling machines. *Nat. Rev. Microbiol.* 14, 33–44.

Otwinowski, Z., and Minor, W. (1997). [20] Processing of X-ray diffraction data collected in

500 oscillation mode (Elsevier).

501 Ozelius, L.J., Hewett, J.W., Page, C.E., Bressman, S.B., Kramer, P.L., Shalish, C., de Leon, D.,
502 Brin, M.F., Raymond, D., Corey, D.P., et al. (1997). The early-onset torsion dystonia gene
503 (DYT1) encodes an ATP-binding protein. *Nat. Genet.* 17, 40–48.

504 Rose, A.E., Brown, R.S.H., and Schlieker, C. (2015). Torsins: not your typical AAA+ ATPases.
505 *Crit. Rev. Biochem. Mol. Biol.* 50, 532–549.

506 Sauer, R.T., and Baker, T.A. (2011). AAA+ proteases: ATP-fueled machines of protein
507 destruction. *Annu. Rev. Biochem.* 80, 587–612.

508 Sosa, B.A., Demircioglu, F.E., Chen, J.Z., Ingram, J., Ploegh, H.L., and Schwartz, T.U. (2014).
509 How lamina-associated polypeptide 1 (LAP1) activates Torsin. *Elife* 3, e03239.

510 Söding, J., Biegert, A., and Lupas, A.N. (2005). The HHpred interactive server for protein
511 homology detection and structure prediction. *Nucleic Acids Res.* 33, W244–W248.

512 Turner, E.M., Brown, R.S.H., Laudermitch, E., Tsai, P.-L., and Schlieker, C. (2015). The Torsin
513 Activator LULL1 Is Required for Efficient Growth of Herpes Simplex Virus 1. *J. Virol.* 89, 8444–
514 8452.

515 Tusnády, G.E., and Simon, I. (2001). The HMMTOP transmembrane topology prediction server.
516 *Bioinformatics* 17, 849–850.

517 Vander Heyden, A.B., Naismith, T.V., Snapp, E.L., Hodzic, D., and Hanson, P.I. (2009). LULL1
518 retargets TorsinA to the nuclear envelope revealing an activity that is impaired by the DYT1
519 dystonia mutation. *Mol. Biol. Cell* 20, 2661–2672.

520 Vulinovic, F., Lohmann, K., Rakovic, A., Capetian, P., Alvarez-Fischer, D., Schmidt, A.,
521 Weißbach, A., Erogullari, A., Kaiser, F.J., Wieggers, K., et al. (2014). Unraveling cellular
522 phenotypes of novel TorsinA/TOR1A mutations. *Hum. Mutat.* 35, 1114–1122.

523 Waterhouse, A.M., Procter, J.B., Martin, D.M.A., Clamp, M., and Barton, G.J. (2009). Jalview
524 Version 2--a multiple sequence alignment editor and analysis workbench. *Bioinformatics* 25,
525 1189–1191.

526 Wendler, P., Ciniawsky, S., Kock, M., and Kube, S. (2012). Structure and function of the AAA+
527 nucleotide binding pocket. *Biochim. Biophys. Acta* 1823, 2–14.

528 White, S.R., and Lauring, B. (2007). AAA+ ATPases: achieving diversity of function with
529 conserved machinery. *Traffic* 8, 1657–1667.

530 Zeymer, C., Barends, T.R.M., Werbeck, N.D., Schlichting, I., and Reinstein, J. (2014). Elements
531 in nucleotide sensing and hydrolysis of the AAA+ disaggregation machine ClpB: a structure-
532 based mechanistic dissection of a molecular motor. *Acta Crystallogr. D Biol. Crystallogr.* 70,
533 582–595.

534 Zhao, C., Brown, R.S.H., Chase, A.R., Eisele, M.R., and Schlieker, C. (2013). Regulation of
535 Torsin ATPases by LAP1 and LULL1. *Proc. Natl. Acad. Sci. U.S.A.* 110, E1545–E1554.

Zhu, L., Wrabl, J.O., Hayashi, A.P., Rose, L.S., and Thomas, P.J. (2008). The torsin-family AAA+ protein OOC-5 contains a critical disulfide adjacent to Sensor-II that couples redox state to nucleotide binding. *Mol. Biol. Cell* 19, 3599–3612.

Zhu, L., Millen, L., Mendoza, J.L., and Thomas, P.J. (2010). A unique redox-sensing sensor II motif in TorsinA plays a critical role in nucleotide and partner binding. *J. Biol. Chem.* 285, 37271–37280.

Zirn, B., Grundmann, K., Huppke, P., Puthenparampil, J., Wolburg, H., Riess, O., and Müller, U. (2008). Novel TOR1A mutation p.Arg288Gln in early-onset dystonia (DYT1). *J. Neurol. Neurosurg. Psychiatr.* 79, 1327–1330.

Figure 1. Architecture of the TorsinA-LULL1 complex.

(A) Schematic diagrams of TorsinA and LULL1. Important residues and sequence motifs are indicated. The colored areas mark the crystallized segments. Large and small domains of TorsinA are colored in purple and pink, respectively. SS, signal sequence; H, hydrophobic region; TM, transmembrane helix. (B) Cartoon representation of the TorsinA-LULL1 complex in two orientations. Color-coding as in (A). A nanobody (VHH-BS2, grey; complementarity determining regions, red) was used as a crystallization chaperone. Numbers refer to secondary structure elements. (C) Close-up of the ATP binding site. Key residues are labeled. $2F_o - F_c$ electron density contoured at 2σ displayed as grey mesh. (D) Close-up of the proximal cysteines 280 and 319 next to the adenine base of the bound ATP. $2F_o - F_c$ electron density is contoured at 1σ . The cysteine pair adopts three alternate conformations, but remains reduced in all of them.

Figure 2. Analysis of the TorsinA-LULL1 interface.

(A) Side-by-side comparison of TorsinA-ATP-LULL1 (left) and TorsinA Δ E-ATP-LULL1 (right). Zoomed insets show the atomic details of the interactions between TorsinA/TorsinA Δ E and LULL1, with a focus on the Δ E303 area. (B and C) Mutational analysis of the TorsinA-LULL1 interface. Substitution or deletion of residues involved in TorsinA-LULL1 binding were probed using a Ni-affinity co-purification assay with recombinant, bacterial-expressed protein. Only TorsinA is His-tagged. SDS-PAGE analysis is shown. Lack of binding is observed by the absence of complex (uncomplexed His-tagged TorsinA is insoluble). t, total lysate, e, Ni eluate. Asterisk denotes an unrelated contaminant.

Figure 3. Oligomerization of TorsinA-LULL1.

(A) Left, Schematic representation of a hypothetical heterohexameric (TorsinA-LULL1)₃ ring model, in analogy to canonical AAA+ ATPases. White star represents ATP. Since LULL1 cannot bind a nucleotide, there would be three catalytic (nucleotide-bound) and three non-catalytic interfaces per ring. Open-book representation of the catalytic interface between TorsinA and LULL1, as seen in this study. Black line marks the outline of the interface. Color gradient marks conservation across diverse eukaryotes. (B) The same analysis as in (A), but for the hypothetical 'non-catalytic' interface. The interface model on the right is based on swapping the TorsinA and LULL1 positions in the TorsinA-LULL1 complex.

Figure 1 – figure supplement 1. Structure comparisons.

(A) Human TorsinA-ATP (left) displayed as a cartoon, compared to the D2 domain of the double-ringed AAA+ ATPase ClpB-AMPPCP (right) from *Thermus thermophilus* (Zeymer et al., 2014) (PDB code 4LJ9) in the same orientation. Important structure motifs are labeled. (B) Human LULL1 (orange) superposed on human LAP1 (grey, PDB code 4TVS), shown in two orientations. The one region of major structural difference is labeled (left). The disulfide bridge within LAP1/LULL1 is in yellow (right).

Figure 1 – figure supplement 2. Phylogenetic analysis of Torsins.

Maximally diverged torsins are aligned. Secondary structure elements of human TorsinA are displayed above the alignment. Important sequence motifs are boxed. LULL1 contacts, red circles, conserved cysteines, yellow circles. Proximal cysteines 280 and 319 connected with a dashed yellow line. Asterisk denotes putative torsin homologs based on sequence analysis. hs, *Homo sapiens*; oa, *Ornithorhynchus anatinus*; gg, *Gallus gallus*; tr, *Takifugu rubripes*; dr, *Danio rerio*; nv, *Nematostella vectensis*; bf, *Branchiostoma floridae*; stp, *Strongylocentrotus*

purpuratus; ci, *Ciona intestinalis*; ce, *Caenorhabditis elegans*; dm, *Drosophila melanogaster*; ta, *Trichoplax adherens*.

Figure 1 – figure supplement 3. Phylogenetic analysis of LAP1/LULL1.

Maximally diverged LAP1 and LULL1 sequences are aligned. If not experimentally confirmed, sequences were assigned as LAP1 or LULL1 based on the presence of an N-terminal, extraluminal domain with basic signature, characteristic of LAP1. Secondary structure elements of human LULL1 are displayed above the alignment. The strictly conserved Arg-finger is boxed. TorsinA contacts, red circles, conserved cysteines, yellow circles. Disulfide bridge depicted as a yellow line. hs, *Homo sapiens*; oa, *Ornithorhynchus anatinus*; gg, *Gallus gallus*; tr, *Takifugu rubripes*; dr, *Danio rerio*; nv, *Nematostella vectensis*; bf, *Branchiostoma floridae*; stp, *Strongylocentrotus purpuratus*; ci, *Ciona intestinalis*; ce, *Caenorhabditis elegans*; dm, *Drosophila melanogaster*; ta, *Trichoplax adherens*.

Figure 1 – figure supplement 4. Nanobody interaction.

The heterotrimeric TorsinA(ATP)-LULL1-VHH-BS2 complex is shown in two orientations. Nanobody and interacting secondary structure elements of TorsinA and LULL1 are shown in full color, non-interacting elements in faded colors. Complementarity determining region (CDR) loops in red. Insets show close-ups with important interacting residues labeled.

Figure 1 – figure supplement 5. Comparison of sequence motifs of AAA+ ATPases.

Torsins and LAP1/LULL1 sequences are compared to the HCLR clade, the most similar branch within the AAA+ ATPase family (Erzberger and Berger, 2006; Iyer et al., 2004). Sequence elements characteristic for each of the 3 groups are displayed as WebLogos (Crooks et al., 2004). Numbering refers to ClpB-D2 from *Thermus thermophilus* for the HCLR class, human

TorsinA for Torsins, and human LULL1 for LAP1/LULL1. Grey bars indicate the characteristic motif or residue, surrounded by a few adjacent residues to emphasize the distinct conservation. All three groups have elements that can be used to distinguish them among each other. Since Torsins and LAP1/LULL1 lack a pore loop consensus sequence $\phi\phi G$ (where ϕ denotes a bulky hydrophobic residue), putative pore loop areas have been determined structurally. Dashed grey bars indicate residues which can be structurally aligned to the pore loop motif of the closest HCLR AAA+ clade members.

Figure 2 – figure supplement 1. Structural mapping of mutations causing dystonia.

All known point mutations and deletions that lead to dystonia are marked as green dots and shown in light green color, respectively, on the TorsinA-ATP-LULL1 structure. A modifier TorsinA mutation, D216H, is marked as a blue dot. The structural equivalent of the LAP1 missense mutation (E482A) is LULL1 E368A, marked as a green dot. See Table 2 for an explanation of the likely structural consequence.

Table 1. X-ray data collection and refinement statistics.

	TorsinA-LULL1 ₂₃₃₋₄₇₀	TorsinAΔE-LULL1 ₂₃₃₋₄₇₀
PDB Code	5J1S	5J1T
Data collection		
Space group	P2 ₁ 2 ₁ 2 ₁	P2 ₁ 2 ₁ 2 ₁
Cell dimensions ^{□□}		
<i>a</i> , <i>b</i> , <i>c</i> (Å)	75.7, 90.7, 105.1	75.5, 88.1, 105.4
α , β , γ (°)	90.0, 90.0, 90.0	90.0, 90.0, 90.0
Resolution (Å)	61 – 1.40 (1.45 – 1.40) ^a	68 – 1.40 (1.45 – 1.40)
<i>R</i> _{sym}	0.06 (0.88)	0.10 (1.98)
<i>R</i> _{pim}	0.03 (0.43)	0.03 (0.60)
<i>I</i> / σ	33.0 (1.5)	30.8 (1.3)
Completeness (%)	94.7 (67.5)	97.9 (96.5)
Redundancy	5.7 (4.4)	12.4 (11.3)
CC(1/2)	1.00 (0.65)	1.00 (0.58)
Refinement		
Resolution (Å)	61.4 – 1.40	67.7 – 1.40
No. reflections	132956	134333
<i>R</i> _{work} / <i>R</i> _{free}	0.142/0.188	0.148/0.177
No. atoms	5898	5927
Protein	5241	5244
Ligand/ion	35	47
Water	622	636
<i>B</i> factors (Å ²)		
Protein	31.3	24.0
Ligand/ion	23.2	17.2
Water	43.1	33.6
r.m.s. deviations		
Bond lengths (Å)	0.014	0.017
Bond angles (°)	1.25	1.71
Ramachandran		
Favored/allowed/outliers (%)	98.0/1.7/0.0	98.6/1.4/0.0

^aValues in parentheses are for highest-resolution shell. One crystal was used for each dataset.

681 **Table 2. Dystonia mutations.**
682
683

Protein	Mutation	Structural consequence	Reference
TorsinA	ΔE302/303	Weakened LAP1/LULL1 binding	(Ozelius et al., 1997)
TorsinA	ΔF323-Y328	Weakened LAP1/LULL1 binding	(Leung et al., 2001)
TorsinA	R288Q	Weakened LAP1/LULL1 binding	(Zirn et al., 2008)
TorsinA	F205I	Folding problem	(Calakos et al., 2010)
TorsinA	D194V	Change to the conserved, noncatalytic interface	(Cheng et al., 2014)
TorsinA	ΔA14-P15	Improper cellular targeting	(Vulinovic et al., 2014)
TorsinA	E121K	Charge inversion at the membrane proximal interface	(Vulinovic et al., 2014)
TorsinA	V129I	Folding problem	(Dobričić et al., 2015)
TorsinA	D216H (modifier)	Surface change; consequence unclear	(Kamm et al., 2008; Kock et al., 2006)
LAP1	c.186delG (p.E62fsTer25)	Lack of the luminal activation domain of LAP1	(Kayman-Kurekci et al., 2014)
LAP1	E482A*	Improper folding	(Dorboz et al., 2014)

684 *Assesment based on the equivalent residue in LULL1 (E368).
685

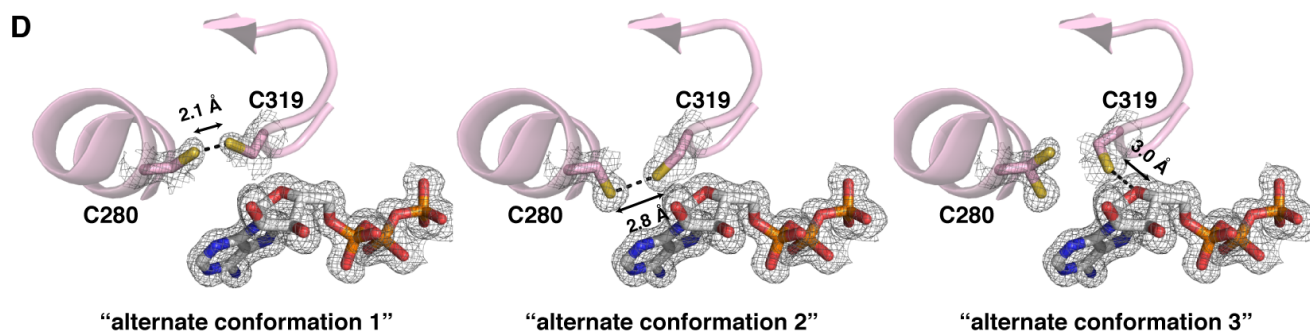
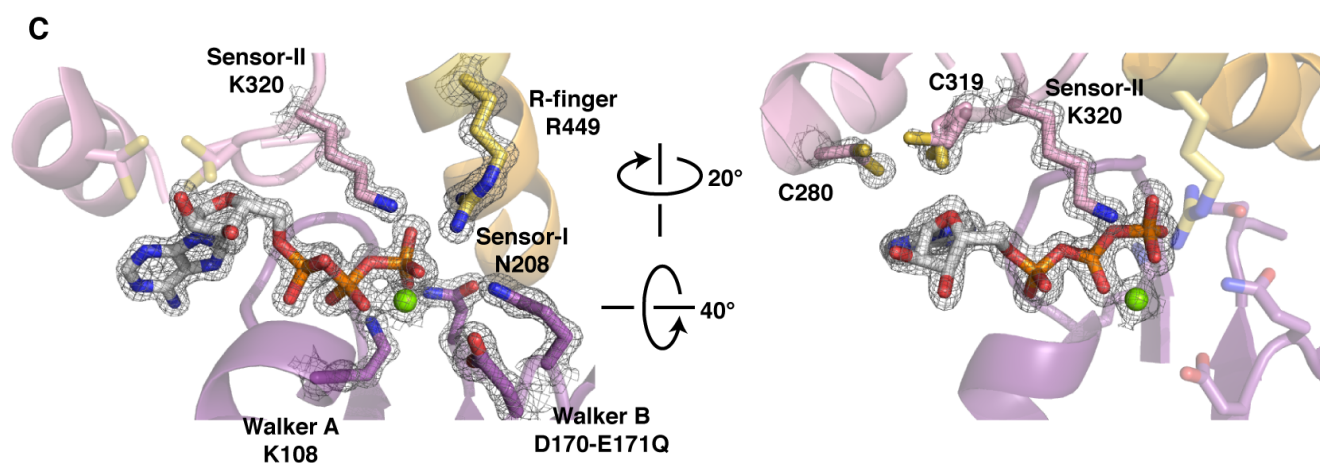
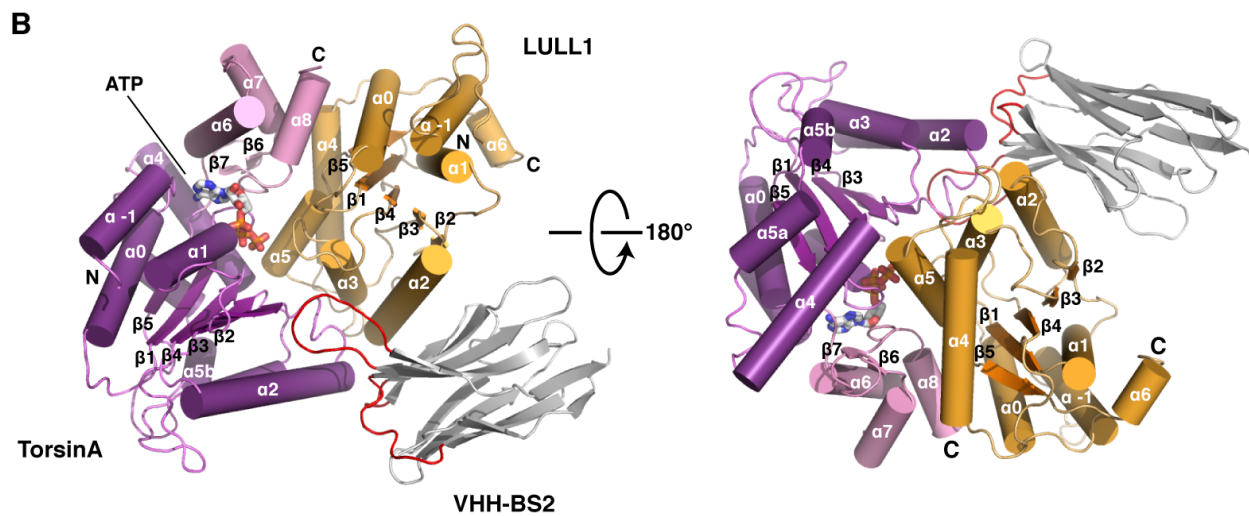
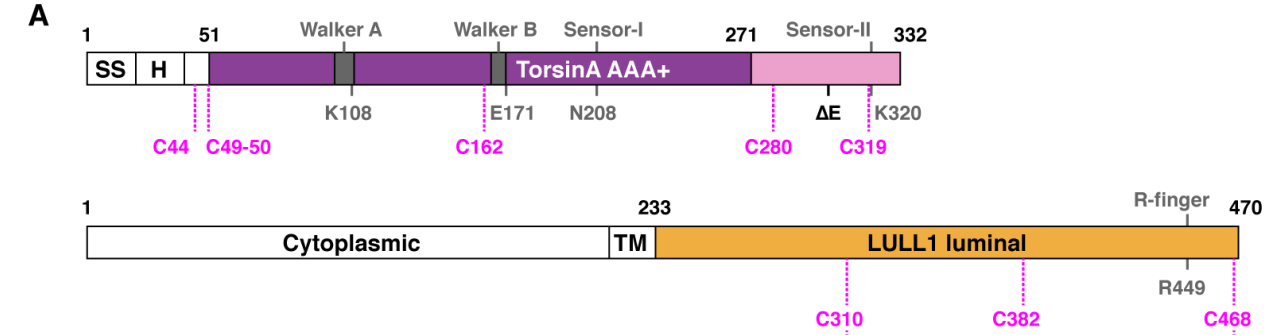


Figure 1

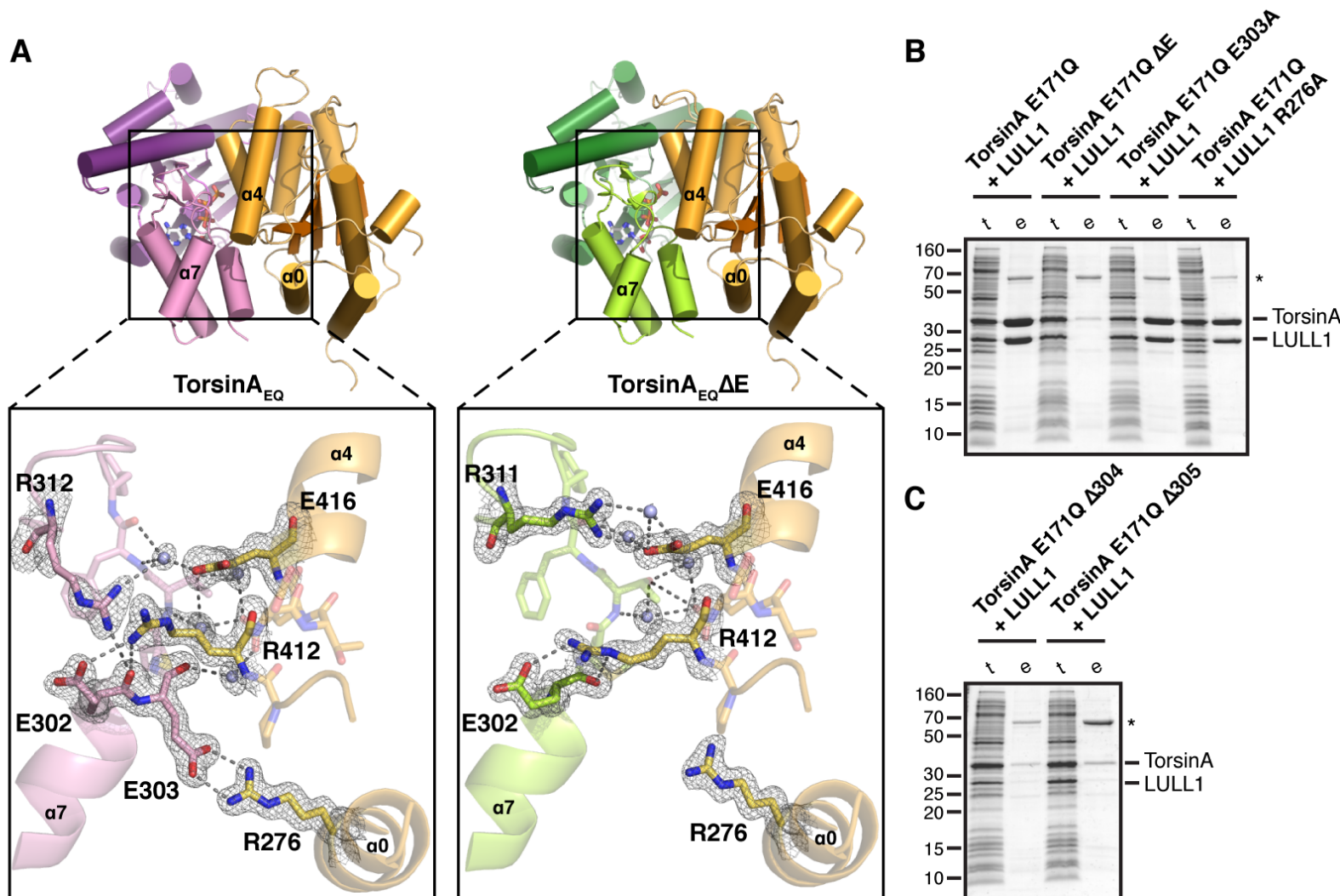


Figure 2

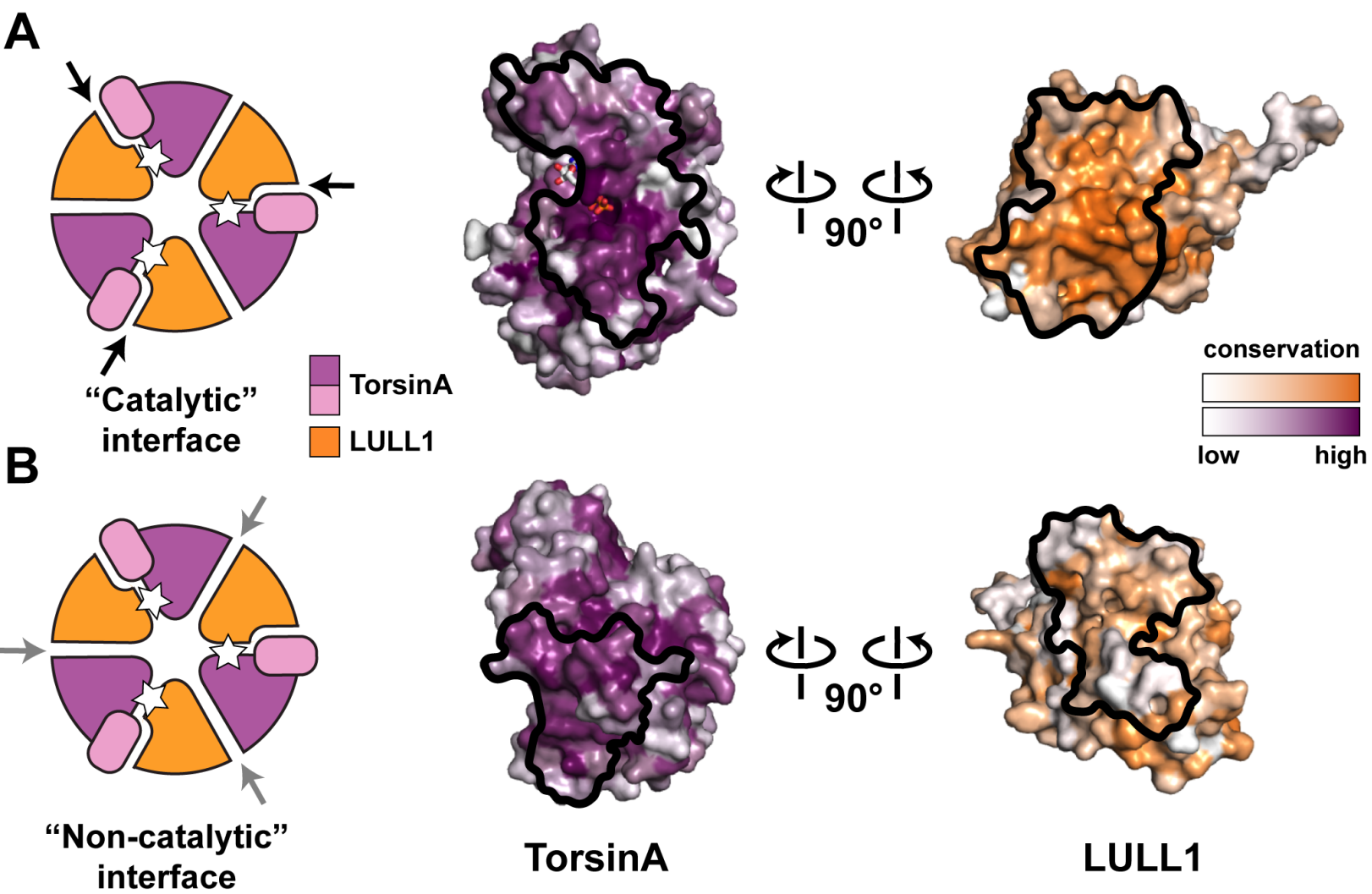


Figure 3